VISUAL SERVOING CONTROLLER FOR ROBOT MANIPULATORS

Jaime Cid and Fernando Reyes

Vicerrectoría de Investigación y Estudios de Posgrado, Grupo de Robótica
Benemérita Universidad Autónoma de Puebla, Facultad de Ciencias de la Electrónica
Apartado Postal 542, Puebla 72001, México

Abstract: This paper presents a new family of fixed-camera visual servoing for planar robot manipulators. The methodology is based on energy-shaping framework in order to derive regulators for position-image visual servoing. The control laws have been composed by the gradient of an artificial potential energy plus a nonlinear velocity feedback. For a static target we characterize the global closed loop attractor using the dynamic robot and vision model, and prove global asymptotic stability of position error for the control scheme, the so called position-based visual servoing. Inverse kinematics is used to obtain the angles of the desired joint, and those of the position joint from computed centroid. Experimental results on a two degrees of freedom direct drive manipulator are presented.

1 INTRODUCTION

The positioning problem of robot manipulators using visual information has been an area of research over the last 30 years. In recent years, attention to this subject has drastically grown. The visual information into feedback loop can solve many problems that limit applications of current robots: automatic driving, long range exploration, medical robotics, aerial robots, etc.

Visual servoing is referred to closed-loop position control for a robot end-effector using direct visual feedback (Hutchinson, 1996). This term was introduced by Hill and Park (Hill, 19179). It represents an attractive solution to position and motion control of autonomous robot manipulators evolving in unstructured environments.

On visual-servoing Weiss *et al.* (Weiss, 1987) and Wilson *et al.* (Wilson, 1996) have categorized two broad classes of vision-based robot control: position-based visual servoing, and image-based visual servoing. In the former, features are extracted from an image and used to estimate the position and orientation of the target with respect to the camera. Using these values, an error signal between the current and the desired position of the robot is defined in the joint space; while in the latter the error signal is defined directly in terms of image features to control the robot end-effector in order to move the image plane feature measurements to a set of desired locations. In both classes of methods, object feature points are mapped onto the camera image plane, and measurements of these points, for example a particularly useful class of image features are centroid used for robot control (Weiss, 1987; Wilson, 1996, Kelly, 1996).

In the configuration between camera and robot, a fixed-camera or a camera-in-hand can be fastened. Fixed-camera robotic systems are characterized in that a vision system fixed in the world coordinate frame, captures images of both the robot and its environment. The control objective of this approach is to move the robot end-effector in such a way that it reaches a desired target. In the camera-in-hand configuration, often called an eye-in-hand, generally a camera is mounted in the robot end-effector and provides visual information of the environment. In this configuration, the control objective is to move the robot end-effector in such a way that the projection of the static target be always at a desired location in the image given by the camera.

Since the first visual servoing systems were reported in the early 1980s the last few years have seen an increase in published research results. An excellent overview of the main issues in visual servo control of robot manipulators is given by (Corke, 1993). However, few rigorous results have been obtained incorporating the nonlinear robot dynamics. The first explicit solution of the problem formulated in this pa-

per was due to Miyazaki and Masutani in 1990, where a control scheme delivers bounded control actions belonging to the Transpose Jacobian-based family, philosophy first introduced by (Takegaki and Arimoto, 1981). Kelly addresses the visual servoing of planar robot manipulators under the fixed-camera configuration in (Reyes, 1998). Malis *et al* (1999) proposed a new approach to vision-based robot control, called 2-1/2-D visual servoing (Malis, 2005). The visual servoing problem is addressed by coupling the nonlinear control theory with a convenient representation of the visual information used by the robot in by (Conticelli, 2001).

(Park and Lee, 2003) present in a visual servoing control for a ball on a flat plate to track its desired trajectory. It has bee proposed in (Kellym 1996) a novel approach, they address the application of the velocity field control philosophy to visual servoing of the robot manipulator under a fixed-camera configuration. Schramm *et al* present a novel visual servoing approach, aimed at controlling the so-called extended-2D (E2D) coordinates of the points constituting a tracked target and provide simulation results (Reyes, 1997). Malis and Benhimane (2005) present a generic and flexible system for vision-based robot control. their system integrates visual tracking and visual servoing approaches in a unifying framework (Malis, 2003).

In this paper we address the positioning problem with fixed-camera configuration to position-based visual servoing of planar robot manipulators. Our main contribution is the development of a new family of position-based visual controllers supported by rigorous local asymptotic stability analysis, taking into account the full nonlinear robot dynamics, and the vision model. The objective concerning the control is defined in terms of joint coordinates which are deduced from visual information. In order to show the performance of the proposed family, two members have been experimentally tested on a two-degree-of-freedom direct drive vertical robot arm.

This paper is organized as follows. In Section 2, we present the robotic system model, the vision model and the formulation of the control problem, then the proposed visual controller is introduced and analyzed. Section 3 presents the experimental set-up. The experimental results are described in Section 4. Finally, we offer some conclusions in Section 5.

2 ROBOTIC SYSTEM MODEL

The robotic system considered in this paper is composed by a direct drive robot and a CCD-camera placed in the robot workspace in the fixed-camera configuration.

2.1 Robot Dynamics

The dynamic model of a robot manipulator plays an important role for simulation of motion, analysis of manipulator structures, and design of control algorithms. The dynamic equation of a *n* degrees of freedom robot in agreement with the Euler-Lagrange methodology (Spong, 1989), is given for

$$M(\mathbf{q})\ddot{\mathbf{q}} + C(\mathbf{q},\dot{\mathbf{q}})\dot{\mathbf{q}} + g(\mathbf{q}) = \tau \qquad (1)$$

where $\mathbf{q}$ is the $n \times 1$ vector of joint displacements, $\dot{\mathbf{q}}$ is the $n \times 1$ vector of joint velocities, τ is the $n \times 1$ vector of applied torques, $M(\mathbf{q})$ is the $n \times n$ symmetric positive definite manipulator inertia matrix, $C(\mathbf{q},\dot{\mathbf{q}})$ is the $n \times n$ matrix of centripetal and Coriolis torques, and $g(\mathbf{q})$ is the $n \times 1$ vector of gravitational torques.

It is assumed that the robot links are joined together with revolute joints. Although the equation of motion (1) is complex, it has several fundamental properties which can be exploited to facilitate the control system design. For the new control scheme, the following important property is used:

Property 1. The matrix $C(\mathbf{q},\dot{\mathbf{q}})$ and the time derivative $\dot{M}(\mathbf{q})$ of the inertia matrix both satisfy [12]:

$$\dot{\mathbf{q}}^T \left[\frac{1}{2}\dot{M}(\mathbf{q}) - C(\mathbf{q},\dot{\mathbf{q}}) \right] \dot{\mathbf{q}} = \mathbf{0} \ \forall \ \mathbf{q}, \dot{\mathbf{q}} \in \mathbb{R}^n. \qquad (2)$$

2.1.1 Model of Direct Kinematic

Direct kinematics is a vectorial function that relate joint coordinates with Cartesian coordinates f: $\mathbb{R}^n \to \mathbb{R}^m$ where *n* is the number of degrees of freedom, and *m* represents the dimension of the Cartesian coordinate frame.

The position $x_R \in \mathbb{R}^3$ of the end-effector with respect to the robot coordinate frame in terms of the joint positions is given by: $x_R = f(\mathbf{q})$.

2.2 Vision Model

The goal of a machine vision system is to create a model of the real world from images. A machine vision system recovers useful information on a scene from its two-dimensional projections. Since images are two-dimensional projections of the three-dimensional world, this recovery requires the inversion of a many-to-one mapping (see Figure 1).

Let $\Sigma_R = \{R_1, R_2, R_3\}$ be a Cartesian frame attached to the robot base, where the axes R_1, R_2 and R_3
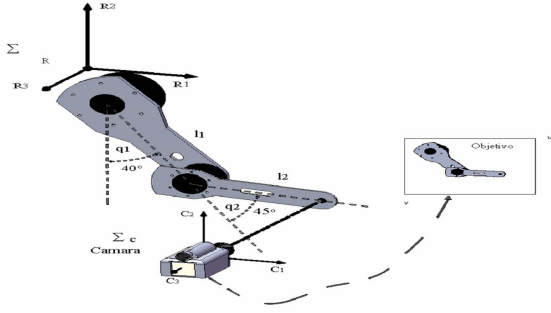
Figure 1: Fixed camera configuration.

represent the robot workspace. A CCD type camera has a $\Sigma_C = \{C_1, C_2, C_3\}$ Cartesian frame, whose origin is attached at the intersection of the optical axis with respect the geometric center of Σ_C. The description of a point in the camera frame is denoted by x_C. The position of the camera frame with respect to Σ_R is denoted by $o_C = [o_{C_1}, o_{C_2}, o_{C_3}]^T$.

The acquired scene is projected on to the CCD. To obtain the coordinates of the image at the CCD plane a perspective transformation is required. We consider that the camera has a perfect aligned optical system and free of optical aberrations, therefore the optical axis intersects at the geometric center of the CCD plane. Finally the image of the scene on the CCD is digitalized, transferred to the computer memory and displayed on the computer screen. We define a new two dimensional computer image coordinate frame $\Sigma_D = \{u, v\}$, whose origin is attached to the upper left corner of the computer screen. Therefore the vision system model is given by:

$$\left[\begin{array}{c} u \\ v \end{array} \right] = \frac{\lambda}{\lambda + x_{C_3}} \left[\begin{array}{cc} \alpha_u & 0 \\ 0 & -\alpha_v \end{array} \right] \left[\begin{array}{c} x_{C_1} \\ x_{C_2} \end{array} \right] \quad (3)$$

$$\left[\begin{array}{c} x_{C_1} \\ x_{C_2} \\ x_{C_3} \end{array} \right] = R^T(\theta)[x_R - o_R^c] \quad (4)$$

where $\alpha_u > 0$, $\alpha_v > 0$ are the scale factors in pixels/m, $\lambda > 0$ is the focal length of the camera and $\frac{\lambda}{\lambda + x_{C_3}} < 0$.

2.3 A New Position-based Visual Servoing Scheme for Fixed-camera Configuration

In this section, we present the stability analysis for the position-based visual servoing scheme. The robot task is specified in the image plane in terms of image feature values corresponding to the relative robot

and object positions. It is assumed that the target resides in the plane $R_1 - R_2$, depicted in Figure 2. Let $[u_d \; v_d]^T$ be the desired image feature vector which is assumed to be constant on the computer image frame Σ_D. The desired joints q_d are estimated from inverse kinematic in function of $\left[\begin{array}{cc} u_d & v_d \end{array} \right]^T$.

The control problem in visual servoing for fixed-camera configuration consists in to designing a control law τ in such a way that the actual image feature $\left[\begin{array}{cc} u & v \end{array} \right]^T$ reaches the desired image feature $\left[\begin{array}{cc} u_d & v_d \end{array} \right]^T$ of the target. The image feature error is defined as $\left[\begin{array}{cc} \tilde{u} & \tilde{v} \end{array} \right]^T = \left[\begin{array}{cc} u_d - u & v_d - v \end{array} \right]^T$, therefore the control aim is to assure that $\lim_{t \to \infty} \left[\begin{array}{cc} \tilde{q}_1 & \tilde{q}_2 \end{array} \right]^T = \left[\begin{array}{cc} q_{d_1} - q_1 & q_{d_2} - q_2 \end{array} \right]^T \to 0$. The control problem is solvable if a joint motion q_d exists such that

$$\left[\begin{array}{c} u_d \\ v_d \end{array} \right] = \left[\begin{array}{cc} \frac{\alpha_u \lambda}{\lambda + x_{C_3}} & 0 \\ 0 & \frac{-\alpha_v \lambda}{\lambda + x_{C_3}} \end{array} \right] R(\theta)^T \left(\left[\begin{array}{c} x_{R_1}(q_d) \\ x_{R_2}(q_d) \end{array} \right] - \left[\begin{array}{c} o_{R_1}^c \\ o_{R_2}^c \end{array} \right]^T \right). \quad (5)$$

In order to solve the visual servoing control problem, we present the next control scheme with gravity compensation:

$$\tau = \nabla v_a(k_p, \widetilde{\mathbf{q}}) - f_v(k_v, \dot{\mathbf{q}}) + g(\mathbf{q}) \quad (6)$$

where $\widetilde{\mathbf{q}} = \mathbf{q}_d - \mathbf{q} \in \mathbb{R}^n$ is the position error vector, $\mathbf{q}_d \in \mathbb{R}^n$ is the desired joint position vector $K_p \in \mathbb{R}^{n \times n}$ is the proportional gain which is a diagonal matrix, $K_v \in \mathbb{R}^{n \times n}$ is a positive definite matrix, also called derivative gain, $\nabla v_a(k_p, \widetilde{\mathbf{q}})$ represents the artificial potential energy, being a positive definite function, and $f_v(k_v, \dot{\mathbf{q}})$ denotes the damping function, which is a dissipative function, that is, $\dot{q}^T f_v(k_v, \dot{\mathbf{q}}) > 0$.

Proposition. Consider the robot dynamic model (1) together with the control law (6), then the closed-loop system is global asymptotically stable, and the visual positioning aim

$\lim_{t \to \infty} \left[\begin{array}{cc} \tilde{q}_1(t) & \tilde{q}_2(t) \end{array} \right]^T = \mathbf{0} \in \mathbb{R}^2$ is achieved.

Proof: The closed-loop system equation obtained by combining the robot dynamic model (1) and control scheme (6) can be written as

$$\frac{d}{dt} \left[\begin{array}{c} \widetilde{\mathbf{q}} \\ \dot{\mathbf{q}} \end{array} \right] = \left[\begin{array}{c} -\dot{\mathbf{q}} \\ M(\mathbf{q})^{-1} \left[\begin{array}{c} \nabla v_a(\mathbf{k_p}, \widetilde{\mathbf{q}}) - \mathbf{f_v}(\mathbf{k_v}, \dot{\mathbf{q}}) \\ -C(\mathbf{q}, \dot{\mathbf{q}})\dot{\mathbf{q}} \end{array} \right] \end{array} \right] \quad (7)$$

which is an autonomous differential equation, and the origin of the state space is a equilibrium point. To carry out the stability analysis of equation (7), the following Lyapunov function candidate is proposed:

$$V(\widetilde{\mathbf{q}}, \dot{\mathbf{q}}) = \frac{1}{2}\dot{\mathbf{q}}^T M(\mathbf{q})\dot{\mathbf{q}} + \upsilon_a(\mathbf{k_p}, \widetilde{\mathbf{q}}). \qquad (8)$$

The first term of $V(\widetilde{\mathbf{q}}, \dot{\mathbf{q}})$ is a positive definite function with respect to $\dot{\mathbf{q}}$ because $M(\mathbf{q})$ is a positive definite matrix. The second one of the Lyapunov function candidate (8), can be interpreted as a potential energy induced by the control law, and is also a positive definite function with respect to the position error $\widetilde{\mathbf{q}}$, because the term $\mathbf{k_p}$ is a positive definite matrix. Therefore, $V(\widetilde{\mathbf{q}}, \dot{\mathbf{q}})$ is both a positive definite and radially unbounded function.

The time derivative of the Lyapunov function candidate (8) along the trajectories of the closed-loop equation (7), and after some algebra and considering property 1, can be written as

$$
\begin{aligned}
\dot{V}(\widetilde{\mathbf{q}}, \dot{\mathbf{q}}) &= \dot{\mathbf{q}}^T M(\mathbf{q})\ddot{\mathbf{q}} - \frac{1}{2}\dot{\mathbf{q}}^T \dot{M}(\mathbf{q})\dot{\mathbf{q}} - \nabla \upsilon_a(\mathbf{k_p}, \widetilde{\mathbf{q}})^T \dot{\mathbf{q}} \\
&= \dot{\mathbf{q}}^T \nabla \upsilon_\mathbf{a}(\mathbf{k_p}, \widetilde{\mathbf{q}}) - \dot{\mathbf{q}}^T \mathbf{f_v}(\mathbf{k_v}, \dot{\mathbf{q}}) - C(\mathbf{q}, \dot{\mathbf{q}})\dot{\mathbf{q}} \\
&\quad + \frac{1}{2}\dot{\mathbf{q}}^T \dot{M}(\mathbf{q})\dot{\mathbf{q}} - \nabla \upsilon_a(\mathbf{k_p}, \widetilde{\mathbf{q}})^T \dot{\mathbf{q}} \\
&= -\dot{\mathbf{q}}^T \mathbf{f_v}(\mathbf{k_v}, \dot{\mathbf{q}}) \le 0 \qquad (9)
\end{aligned}
$$

which is a negative semidefinite function and therefore, it is possible to conclude stability in the equilibrium point. In order to prove local asymptotic stability, the autonomous nature of the closed-loop equation (7) is exploited to apply the LaSalle's invariance principle (Khalil, 2002) in the region Ω:

$$
\Omega = \left\{ \begin{array}{c} \begin{bmatrix} \widetilde{\mathbf{q}}_1 \\ \widetilde{\mathbf{q}}_2 \\ \dot{\mathbf{q}} \end{bmatrix} \in \mathbb{R}^{2n} : \dot{V}(\widetilde{\mathbf{q}}, \dot{\mathbf{q}}) = 0 \\ \widetilde{\mathbf{q}} = 0 \in \mathbb{R}^n, \dot{\mathbf{q}} = 0 \in \mathbb{R}^n : \dot{V}(\widetilde{\mathbf{q}}, \dot{\mathbf{q}}) = 0 \end{array} \right\} \quad (10)
$$

since $\dot{V}(\widetilde{\mathbf{q}}, \dot{\mathbf{q}}) \le 0 \in \Omega$, $V(\widetilde{\mathbf{q}}(t), \dot{\mathbf{q}}(t))$ is a decreasing function of t. $V(\widetilde{\mathbf{q}}, \dot{\mathbf{q}})$ is continuous on the compact set Ω, it is bounded from below on Ω. For example, it satisfies $0 \le V(\widetilde{\mathbf{q}}(t), (t), \dot{\mathbf{q}}(t)) \le V(\widetilde{\mathbf{q}}(0), \dot{\mathbf{q}}(0))$. Therefore, the trivial solution is the only solution of the closed-loop system (7) restricted to Ω. Consequently it is concluded that the origin of the state space is locally asymptotically stable.

2.4 Examples of Application

The purpose of this section is to exploit the methodology described above with the objective to derive new regulators.

We present control scheme with gravity compensation:

$$\tau = K_p \tanh\begin{bmatrix} \widetilde{\mathbf{q}}_1 \\ \widetilde{\mathbf{q}}_2 \end{bmatrix} - K_v \tanh\begin{bmatrix} \dot{\mathbf{q}}_1 \\ \dot{\mathbf{q}}_2 \end{bmatrix} + g(q). \qquad (11)$$

Proof: The closed-loop system equation obtained by combining the robot dynamic model (1) and control scheme (7) can be written as

$$\frac{d}{dt}\begin{bmatrix} \widetilde{\mathbf{q}} \\ \dot{\mathbf{q}} \end{bmatrix} = \begin{bmatrix} -\dot{\mathbf{q}} \\ M(\mathbf{q})^{-1} \begin{bmatrix} \mathbf{k_p}\tanh(\widetilde{\mathbf{q}}) - \mathbf{K_v}\tanh(\dot{\mathbf{q}}) \\ -C(\mathbf{q}, \dot{\mathbf{q}})\dot{\mathbf{q}} \end{bmatrix} \end{bmatrix} \quad (12)$$

which is an autonomous differential equation, and the origin of the state space is a equilibrium point. To carry out the stability analysis of equation (12), the following Lyapunov function candidate is proposed:

$$
V(\widetilde{\mathbf{q}}, \dot{\mathbf{q}}) = \frac{1}{2}\dot{\mathbf{q}}^T M(\mathbf{q})\dot{\mathbf{q}} + \sqrt{\ln\left(\cosh\begin{bmatrix} \widetilde{\mathbf{q}}_1 \\ \widetilde{\mathbf{q}}_2 \end{bmatrix}\right)}^T
$$
$$
K_p\sqrt{\ln\left(\cosh\begin{bmatrix} \widetilde{\mathbf{q}}_1 \\ \widetilde{\mathbf{q}}_2 \end{bmatrix}\right)} \qquad (13)
$$

The first term of $V(\widetilde{\mathbf{q}}, \dot{\mathbf{q}})$ is a positive definite function with respect to $\dot{\mathbf{q}}$ because $M(\mathbf{q})$ is a positive definite matrix. The second one of the Lyapunov function candidate (13), can be interpreted as a potential energy induced by the control law, and is also a positive definite function with respect to position error $\widetilde{\mathbf{q}}$, because the term $\mathbf{k_p}$ is a positive definite matrix. Therefore, $V(\widetilde{\mathbf{q}}, \dot{\mathbf{q}})$ is both a positive definite and radially unbounded function.

The time derivative of Lyapunov function candidate (13) along the trajectories of the closed-loop equation (12) and after some algebra and considering property 1, can be written as:

$$
\begin{aligned}
\dot{V}(\widetilde{\mathbf{q}}, \dot{\mathbf{q}}) &= \dot{\mathbf{q}}^T M(\mathbf{q})\ddot{\mathbf{q}} - \frac{1}{2}\dot{\mathbf{q}}^T \dot{M}(\mathbf{q})\dot{\mathbf{q}} - \dot{\mathbf{q}}^T K_p \tanh\begin{bmatrix} \widetilde{\mathbf{q}}_1 \\ \widetilde{\mathbf{q}}_2 \end{bmatrix} \\
&= \dot{\mathbf{q}}^T \tanh\begin{bmatrix} \widetilde{\mathbf{q}}_1 \\ \widetilde{\mathbf{q}}_2 \end{bmatrix} - \dot{\mathbf{q}}^T K_v \tanh\begin{bmatrix} \widetilde{\mathbf{q}}_1 \\ \widetilde{\mathbf{q}}_2 \end{bmatrix} \\
&\quad - C(\mathbf{q}, \dot{\mathbf{q}})\dot{\mathbf{q}} + \frac{1}{2}\dot{\mathbf{q}}^T \dot{M}(q)\dot{\mathbf{q}} - \dot{\mathbf{q}}^T K_p \tanh\begin{bmatrix} \widetilde{\mathbf{q}}_1 \\ \widetilde{\mathbf{q}}_2 \end{bmatrix} \\
&= -\dot{\mathbf{q}}^T K_v \tanh\begin{bmatrix} \dot{\mathbf{q}}_1 \\ \dot{\mathbf{q}}_2 \end{bmatrix} \le 0 \qquad (14)
\end{aligned}
$$

A second example from the proposed methodology:

$$\tau = K_p \arctan\begin{bmatrix} \widetilde{\mathbf{q}}_1 \\ \widetilde{\mathbf{q}}_2 \end{bmatrix} - K_v \arctan\begin{bmatrix} \dot{q}_1 \\ \dot{q}_2 \end{bmatrix} + g(\mathbf{q}). \qquad (15)$$

3 EXPERIMENTAL SET-UP

An experimental system for research of robot control algorithms has been designed and built at the Universidad Autónoma de Puebla, México; it is a direct-drive robot of two degrees of freedom (see Figure 2). The experimental robot consists of two links made of 6061 aluminum actuated by brushless direct-drive servo actuators from Parker Compumotor in order to drive the joints without gear reduction. Advantages of this type of direct-drive actuator includes freedom from backlashes and significantly lower joint friction compared to actuators composed by gear drives. The motors used in the robot are listed in Table 1. The servos are operated in torque mode, so the motors act as a torque source and they accept an analog voltage as a reference of torque signal. Position information is obtained from incremental encoders located on the motors. The standard backwards difference algorithm applied to the joint positions measurements was used to generate the velocity signals. The manipulator workspace is a circle with a radius of 0.7 m. Besides position sensors and motor drivers, the robot also includes a motion control board, manufactured by Precision MicroDynamics Inc., which is used to obtain the joint positions. The control algorithm runs on a Pentium host computer.
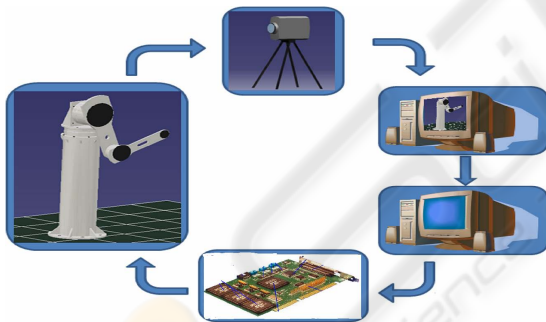

Figure 2: Experimental robot.

Table 1: Servo actuators of the experimental robot.

Link	Model	Torque	p/rev
Shoulder	DM1050A	50	1,024,000
Elbow	DM1004C	4	1,024,000

With reference to our direct-drive robot, only the gravitational torque is required to implement the new control scheme (6), which is available in (Malis, 2005):

$$g(\mathbf{q}) = \begin{bmatrix} 38.46\sin(q_1) + 1.82\sin(q_1+q_2) \\ 1.82\sin(q_1+q_2) \end{bmatrix} \text{ [Nm]}. \tag{16}$$

4 EXPERIMENTAL RESULTS

To support our theoretical developments, this Section presents experimental results of the proposed controllers on a planar robot for the fixed-camera configuration.
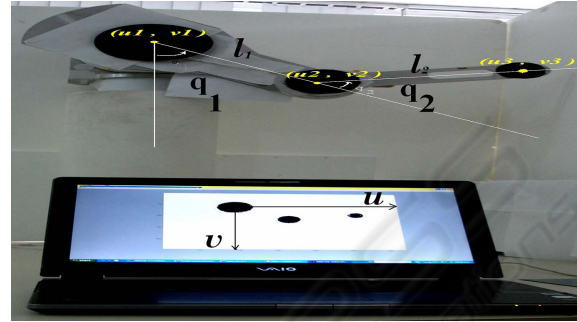

Figure 3: Robot manipulator and vision system.

Three black disks were mounted on the shoulder joint, elbow joint and end-effector, repestively. A big black disk for shoulder, a medium black disk on elbow, and a small one for the end-effector. The joint coordinates were estimated from predictable centroid using inverse kinematics as is shown in Figure (3):

$$l_1 = \sqrt{(u_2-u_1)^2 + (v_2-v_1)^2} \tag{17}$$

$$l_2 = \sqrt{(u_3-u_2)^2 + (v_3-v_2)^2} \tag{18}$$

and

$$q_2 = \arccos\left(\frac{(u_3-u_2)^2 + (v_3-v_2)^2 - l_1^2 - l_2^2}{2l_1l_2}\right) \tag{19}$$

$$q_1 = \left(\frac{\pi}{2}\right) - atan\left(\frac{v_2-v_1}{u_2-u_1}\right) - atan\left(\frac{l_2\sin(q_2)}{l_1+l_2\cos(q_2)}\right) \tag{20}$$

where l_1, l_2 represent the link longitude respectively, u and v are visual information from equations (19) and (20) using in Figure 3.

The centroids of each disc were selected as object feature points. We select in all controllers the desired position in the image plane as $[u_d\ v_d]^T = [198\ 107]^T$ [pixels] and the following initial position $[u(0)\ v(0)]^T = [50\ 210]^T$ [pixels], this $q_1(0), q_2(0) = [0\ 0]^T$ and $\dot{\mathbf{q}}(0) = \mathbf{0}$ [degrees/sec]. The evaluated controllers have been written in C language. The sampling rate was executed at 2.5 ms., while the visual feedback loop was at 33 ms. The CCD camera was placed in front of the robot and its position with respect to the robot frame Σ_R was $O_c^R = [0_{c_1}^R, 0_{c_2}^R, 0_{c_3}^R]^T = [-0.5, -0.6, -1]^T$ meters, the rotation angle $\theta = 0$ degrees. We use MATLAB version 2007a, applying, the

SIMULINK module to carry out the imagine processing. The video signal from the CCD-camera has a resolution of 320x240 pixels in RGB format.

Figures 4 and 5 show the experimental results of the controller (11), the proportional and derivative gains were selected as $K_p = \text{diag}\{26.0, 1.8\}$ [N], $K_v = \text{diag}\{12.0, 1.2\}$ [Nm]. respectively and $\mathbf{u}_d = 198$ y $\mathbf{v}_d = 107$. The transient response with around 3 seconds is fast. The components of the feature position error tend asymptotically close to zero.

The experimental results for the controller (11) are shown in Figures (4) and (5). The transient response was around 3 seconds. The components of the feature position error tend asymptotically.
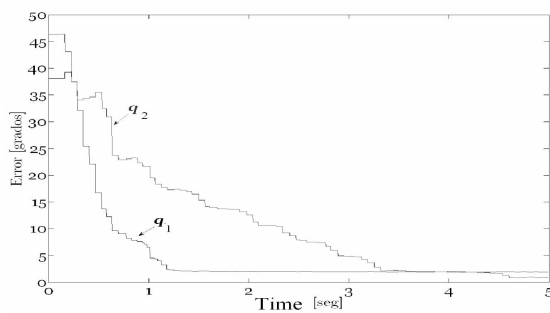

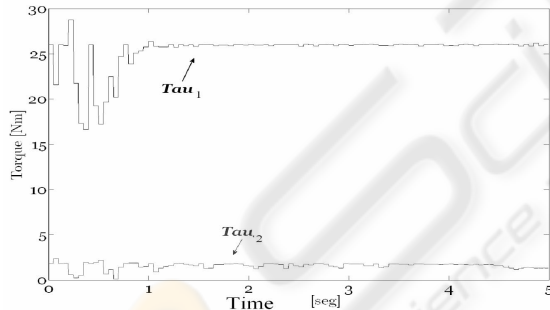Figure 4: Error for controller (11).

Figure 5: Torque for controller tanh.

Figures 6 and 7 show the experimental results of the controller (15). The proportional and derivative gains were selected as $K_p = \text{diag}\{17.3, 1.2\}$ [N], $K_v = \text{diag}\{6.6, 1.2\}$ [Nm], respectively, and $\mathbf{u}_d = 198$ y $\mathbf{v}_d = 107$. The transient response is fast by around 1 second. The components of the feature position error tend asymptotically to a neighborhood close to zero.

The experimental results for the controller (15) are shown in Figures 6 and 7. The transient response was around 1 second. The components of the feature position error tend asymptotically.
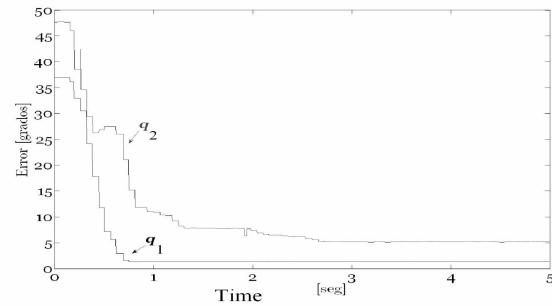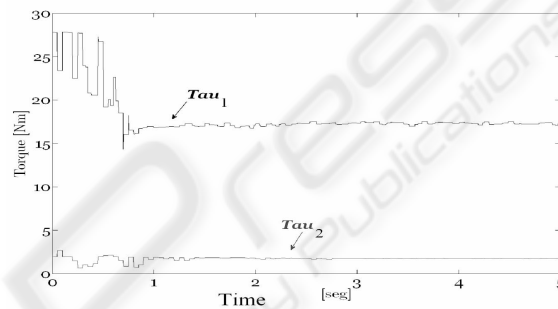

Figure 6: Error for controller (15).

Figure 7: Torque for controller atan.

5 CONCLUSIONS

In this paper we have presented a new methodology to design position-based visual servoing for planar robots in fixed-camera configuration. It should be emphasized both that the nonlinear robot dynamics and the vision model have been included in the stability analysis. The class of controllers are energy-shaping based, and they are described by control laws composed of the gradient of an artificial potential energy plus a linear velocity feedback. Experimental results with a two degrees of freedom planar robot, using three feature points were presented to illustrate the performance of the control scheme.

REFERENCES

Hutchinson S., G. D. Hager and P. I. Corke, *A Tutorial on Visual Servo Control.* IEEE Trans. on Robotics and Automation, Vol. 12, No. 5, October 1996, pp. 651-670.

Hill J. and W. T. Park, *Real Time Control of a Robot with a Mobile Camera.* in Proc. 9th ISIR, Washington, D.C., Mar. 1979, pp. 233-246.

Weiss L. E., A. C. Sanderson, and C. P. Neuman, *Dynamic sensor-based control of robots with visual feedback.*

in IEEE Journal of Robot. Automat., vol. RA-3, pp. 404-417, Oct. 1987.

Wilson W. J., C. C. Williams, and Graham S. B. *Relative End-Effector Control Using Cartesian Position Based Visual Servoing.* IEEE Transactions on Robotics and Automation. vol. 12 No. 5, pp. 684-696. October 1996

Kelly R., P. Shirkey and M. W. Spong, *Fixed-Camera Visual Servo Control for Planar Robots.* IEEE International Conference on Robotics and Automation. Minneapolis, Minnesota, April 1996, pp. 2643-2649.

Corke P. I. *Visual Control of Robot Manipulators A review.* Visual Servoing, K. Hashimoto, Ed. Singapore: World Scientific, pp. 1-31, 1993.

Takegaki M. and S. Arimoto, *A New Feedback Method for Dynamic Control of Manipulators.* ASME J. Dyn. Syst. Meas. Control, Vol. 103, 1981, pp. 119-125.

Malis E. and S. Benhimane, *A Unified Approach to Visual Tracking and Servoing.* Robotics and Autonomous Systems, Vol. 52, Issue 1, 31 July 2005, pp. 39-52.

Conticelli F. and B. Allotta, *Nonlinear Controllability and Stability Analysis of Adaptive Image-Based Systems.* IEEE Trans. on Robotics and Automation, Vol. 17, No. 2, 2001, pp. 208-214.

Park J. and Y.J. Lee, *Robust Visual Servoing for Motion Control of the Ball on a Plate.* Mechatronics, Vol. 13, Issue 7, September 2003, pp. 723-738.

Malis E. and P. Rives, *Robustness of Image-based Visual Servoing with Respect to Depth Distribution Errors.* IEEE International Conference on Robotics and Automation. 2003, pp. 1056-1061.

Spong M. W. and M. Vidyasagar, *Robots Dynamics and Control.* John Wiley & Sons, 1989.

Reyes F. and R. Kelly, *Experimental Evaluation of Fixed-Camera Direct Visual Controllers on a Direct-Drive Robot.* IEEE International Conference on Robotics & Automation. Leuven, Belgium, May 1998, pp. 2327-2332.

Khalil, H. K. (2002). Nonlinear Systems. Prentice–Hall, Upper Saddle River, NJ.

Chen J., A. Behal, D. Dawson and Y. Fang, *2.5D Visual Servoing with a Fixed Camera.* American Control Conference. 2003, pp. 3442-3447.

Schramm F., G. Morel, A. Micaelli and A. Lottin, *Extended-2D Visual Servoing.* IEEE International Conference on Robotics and Automation. 2004, pp. 267-273.

Reyes F. and R. Kelly (1997). Experimental evaluation of identification schemes on a direct drive robot. *Robotica*, Cambridge University Press. Vol. 15, 563–571.